Programmable active kirigami metasheets with more freedom of actuation

Yichao Tang[a,b,1], Yanbin Li[b,1], Yaoye Hong[b], Shu Yang[c], and Jie Yin[a,b,2]

[a]Department of Mechanical Engineering, Temple University, Philadelphia, PA 19122; [b]Department of Mechanical and Aerospace Engineering, North Carolina State University, Raleigh, NC 27695; and [c]Department of Materials Science and Engineering, University of Pennsylvania, Philadelphia, PA 19104

Edited by John A. Rogers, Northwestern University, Evanston, IL, and approved November 15, 2019 (received for review April 15, 2019)

Kirigami (cutting and/or folding) offers a promising strategy to reconfigure metamaterials. Conventionally, kirigami metamaterials are often composed of passive cut unit cells to be reconfigured under mechanical forces. The constituent stimuli-responsive materials in active kirigami metamaterials instead will enable potential mechanical properties and functionality, arising from the active control of cut unit cells. However, the planar features of hinges in conventional kirigami structures significantly constrain the degrees of freedom (DOFs) in both deformation and actuation of the cut units. To release both constraints, here, we demonstrate a universal design of implementing folds to reconstruct sole-cuts–based metamaterials. We show that the supplemented folds not only enrich the structural reconfiguration beyond sole cuts but also enable more DOFs in actuating the kirigami metasheets into 3 dimensions (3D) in response to environmental temperature. Utilizing the multi-DOF in deformation of unit cells, we demonstrate that planar metasheets with the same cut design can self-fold into programmable 3D kirigami metastructures with distinct mechanical properties. Last, we demonstrate potential applications of programmable kirigami machines and easy-turning soft robots.

kirigami | metamaterial | thermal actuation | programmable machine | polarization switch

Mechanical metamaterial is an emerging frontier in scientific research and engineering innovation due to its unique physical properties (1, 2). The paper art, origami (folding) and kirigami (cutting), has recently inspired the creation of a variety of programmable and reconfigurable metamaterials through folding or cutting a thin sheet (3–11). Different from folding into compact 3-dimensional (3D) structures in origami (12–16), opening of cuts in kirigami sheets achieves highly expandable and stretchable 2D and 3D structures through either in-plane rigid rotation of cut units or out-of-plane buckling of the struts between cuts (8, 9, 17–22). Such in-plane and out-of-plane deformation in kirigami sheets are tunable by manipulating the geometry of the hinges between cuts (17), which has broad applications ranging from stretchable electronics to soft machines (18, 20, 23–27).

However, both cut-opening mechanisms for structure reconfiguration in kirigami sheets have intrinsic limitations: in 2D kirigami, there exists a maximally expanded configuration achieved by in-plane rotation for any cut pattern, i.e., a polarized state, beyond which the structure cannot be further reconfigured (9, 20); in 3D kirigami, uniform spontaneous local buckling in cut units generates a globally periodic and homogenous 3D structure (8, 9, 17–20, 28), lacking control of both localized deformation in cut units and global structure reconfiguration through the sheet.

Here, by combining a universal fold design and line cuts (slits) in a thin flat sheet, we propose a unified cut-opening mechanism, i.e., folding-induced opening of cuts, to overcome the limitations in both 2D and 3D kirigami sheets. We show that as folding is increased, the reconstructed 2D kirigami sheet with implemented folds expands first, bypassing the maximally stretched state in its counterpart of sole-cut–based kirigami sheet, and then even shrinks to its original compact state with cuts reclosed. We demonstrate that the added folds largely release the constrained degree of freedom (DOF) in the hinges, allowing both in-plane (single DOF) and out-of-plane rotation (multiple DOFs) of the cut units through folding, and consequently active manipulation of programmable 2D and 3D shape shifting locally and globally in stimuli-responsive kirigami sheets through self-folding. In contrast to folding of kirigami sheets with excised holes into compact 3D structures through folding-induced closing of cuts (29), we show that kirigami sheets with combined folds and slits realize both compact and expanded structures in 2D and 3D by leveraging folding-induced opening and reclosing of the cuts. Moreover, we demonstrate harnessing folding and rotation in active kirigami structures for potential applications in design of programmable 3D self-folding kirigami machines and soft turning robots.

Results

Folding-Based Reconfigurable Kirigami Metasheets. Fig. 1 *A* and *B* show the schematics of 2 reconstructed basic cut unit cells in a square (Fig. 1 *A*, *i*) and hexagonal (Fig. 1 *B*, *i*) shape with designed folds at the vertices of each line cut. One mountain and 2 valleys are added to the vertices of line cuts to form a tetrahedron hinge. Folding of tetrahedron hinges at the vertices induced by either mechanical stretching (*SI Appendix*, Fig. S1 and Movie S1) or stimuli leads to in-plane or out-of-plane rigid rotation of cut plates depending on the folding angles at the hinges, and thus the pore opening of the line cuts in the unit cells (Fig. 1 *A* and *B*, *ii*), correspondingly the shape transformation in the 2D metasheet consisting of multiple periodic unit cells, e.g., square (Fig. 1 *A*, *iii*) and kagome (Fig. 1 *B*, *iii*) lattice structures.

Geometric Mechanics Model of 2D Kirigami Metasheets. The constructed 2D kirigami metasheet can be treated as being made of identical coplanar rigid square or triangular cut plates connected by a

Significance

Kirigami is an emerging approach to construct 3-dimensional (3D) structures by simply cutting and folding thin sheets. Sole slits lead to expanded 3D structures through buckling to open the cuts. Compared to homogenous shape shifting through thin sheets with sole cuts, adding folds into cuts provides potential for programmable structure reconfiguration in kirigami sheets with excised holes. However, folding often closes the cutouts in such kirigami sheets, resulting in compact 3D pop-up structures. Here, we combine a universal fold design and slits in kirigami sheets to realize both expanded and compact structures, allowing reprogrammability in both 2D and 3D through folding-induced opening and reclosing of slits. We demonstrate thermal actuation of programmable kirigami metastructures and machines through cuts-guided directional folding.

Author contributions: Y.T., S.Y., and J.Y. designed research; Y.T., Y.L., Y.H., and J.Y. performed research; Y.T., Y.L., S.Y., and J.Y. analyzed data; and Y.T., Y.L., S.Y., and J.Y. wrote the paper.

The authors declare no competing interest.

This article is a PNAS Direct Submission.

[1]Y.T. and Y.L. contributed equally to this work.

[2]To whom correspondence may be addressed. Email: jyin8@ncsu.edu.

This article contains supporting information online at https://www.pnas.org/lookup/suppl/doi:10.1073/pnas.1906435116/-/DCSupplemental.

First published December 16, 2019.

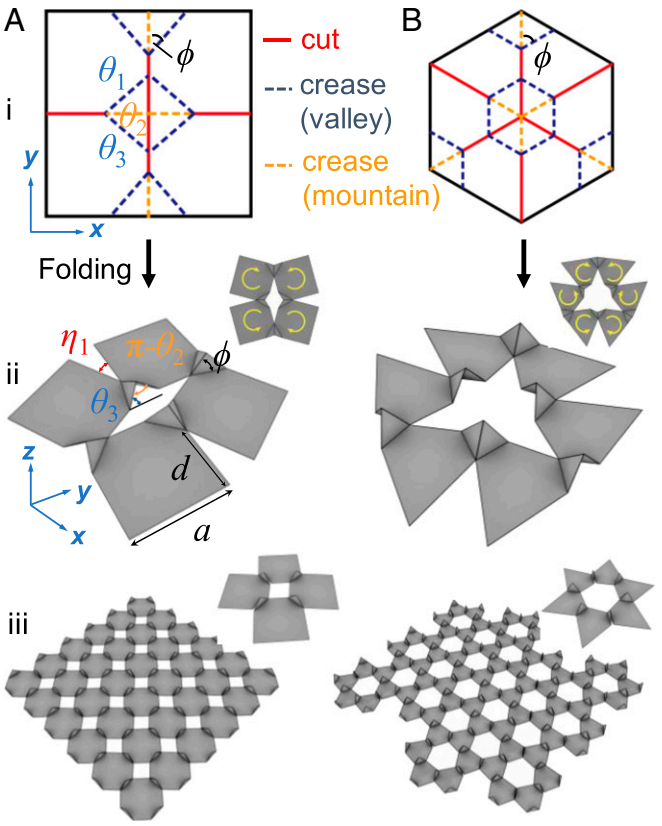

Fig. 1. Two-dimensional reconfigurable kirigami metasheets constructed from combined cuts and folds. (*A* and *B*) Schematic of geometry of a single kirigami unit cell in a square (*A*) and triangular cut (*B*). Three creases (dashed line) are introduced to the vertices of line cuts (red solid line) to form a tetrahedron hinge. Folding of creases leads to the opening of line cuts and the shape shifting in both single and periodic units.

linear elastic tetrahedron hinge at the ridges. Its geometry is parameterized by 2 folding angles, i.e., $\theta_1 = \theta_3 \in [0, \pi/2]$ at the valley and $\theta_2 \in [0, \pi]$ at the mountain, as well as 1 inclined angle $\phi \in [0, \tan^{-1}[1/(1-\bar{d})]]$, where $\bar{d} = d/a$ is the normalized cut length with d being the line cut length and a being the unit cell length (Fig. 1*A* and *SI Appendix*, Figs. S2 and S3). For in-plane rigid rotation of cut plates, it has only one DOF since the folding angles at mountain (θ_2) and valley (θ_1 and θ_3) ridges satisfy the following (*SI Appendix*, Fig. S4):

$$\theta_1 = \theta_3 = sin^{-1}\left[\frac{\sin(\theta_2/2)}{\sqrt{\sin^2\phi\,\sin^2(\theta_2/2)+\cos^2\phi}}\right]. \quad [1]$$

Thus, the unit cell can be fully characterized by θ_2, or equivalently the opening angle η_1 (Fig. 1 *A*, *ii*), satisfying the following:

$$\eta_1 = 2(\phi - \xi) \text{ with } \xi \equiv \sin^{-1}[\sin\phi\cos(\theta_2/2)]. \quad [2]$$

As the mountain crease starts to fold, i.e., θ_2 increases, the cut starts to open and η_1 increases monotonically (*SI Appendix*, Fig. S5). Specifically, when the mountain crease is completely folded, i.e., $\theta_2 = \pi$, Eqs. **1** and **2** become the following:

$$\theta_1 = \theta_3 = \theta_2/2 = \pi/2, \quad \eta_1 = 2\phi. \quad [3]$$

The valley creases have a right-angle fold and the 2 triangular hinged facets become contacted and coplanar perpendicular to the cut plates; thus, η_1 arrives at its maximum opening angle $(\eta_1)_{max} = 2\,\phi$. Consequently, the kirigami sheets exhibit a square lattice pattern for square cut units with $\phi = \pi/4$ (Fig. 1 *A*, *iii*) and a kagome pattern for triangular cut units with $\phi = \pi/3$ (Fig. 1 *B*, *iii*), the structure configurations of which are similar to the maximally expanded patterns of their counterparts with sole cuts (20).

For the metasheet with square cuts, as the hinge folds, the resulting nominal macroscopic strains ε_{xx} and ε_{yy} along x or y direction are as follows (*SI Appendix*):

$$\varepsilon_{xx} = \varepsilon_{yy} \equiv \varepsilon = \bar{d}\,\sin(\eta_1/2) + \cos(\eta_1/2) + (1-\bar{d})\tan\phi[\cos(\theta_2/2) - \cos(\eta_1/2)]. \quad [4]$$

The Poisson's ratio $\nu_0 = -1$ is the same as its counterpart without folds.

Eq. **3** shows that $(\eta_1)_{max}$ can be tuned by manipulating ϕ. This is in sharp contrast to the nontunable value of $(\eta_1)_{max} = 90°$ in its counterpart with sole cuts (20). As demonstrated in Fig. 2*A*, a paper square cut unit cell without folds is manually stretched. When the squares rotate to 45°, it arrives at a maximum opening angle of 90°. It represents a maximally stretched state that cannot be further stretched or rotated due to its infinite stiffness in both x and y directions (9), beyond which the hinge will be broken (Fig. 2*A*). It holds true for any cut patterns for shape shifting through in-plane rotation (20). However, for the paper square cut unit with creases (Fig. 2*B*), in terms of Eq. **2**, by setting $\phi > 45°$ (e.g., $\phi = 75°$), it can readily bypass the maximally stretched state with $(\eta_1)_{max} = 90°$ in its counterpart through folding, and η_1 can be even close to 180° without hinge rupture. Consequently, the unit cell undergoes a structure polarization switch from y axis to x axis (red dashed line in Fig. 2*B*) (9): The center cut opens first, and then recloses as folding increases monotonically, which is impossible to be achieved by its counterparts with sole cuts (9, 20), demonstrating the uniqueness enabled by combined folds and cuts beyond sole cuts. Correspondingly, for large $\phi \geq 45°$, as folding increases, the nominal strain ε in Eq. **4** exhibits a peak by increasing first (expanding) and then dropping to even negative values (shrinking) (Fig. 2 *C*, *Inset*), which is in sharp contrast to the monotonic increase of ε for small ϕ and its counterparts with sole cuts (9, 20).

To better understand the polarization switch behavior in the cut unit cell with folds, we develop a theoretical model to predict its in-plane stretching stiffness under uniaxial stretching (30). The total potential energy Π of the deformed unit cell under uniaxial stretching force F_y can be expressed as follows (*SI Appendix*):

$$\Pi = U - W, \quad U = 4kx_2(\theta_2-\theta_0)^2 + 8kx_4(\alpha-\alpha_0)^2, \quad W = \int_{\theta_0}^{\theta_2} F_y\frac{dl}{d\theta_2}d\theta_2, \quad [5]$$

where U is the elastic energy stored in the linear elastic hinges and W is the potential energy from the external force. k is the hinge spring constant, and $x_2 = a\,(1-\bar{d})$ and $x_4 = a\,(1-\bar{d})/\cos\phi$ are the length of mountain and valley creases, respectively. θ_0 and α_0 are the respective 2 folding angles in undeformed state with $\alpha_0 = sin^{-1}[\cos(\theta_0/2)/\sqrt{\sin^2\phi\cos^2(\theta_0/2)+\cos^2\phi}]$. l is the nominal length of the deformed unit cell. For a randomly selected deformed state, the equilibrium equation under the applied force can be obtained by minimizing Π, i.e., $\delta\Pi/\delta\theta_2 = 0$. The stretching stiffness K_y along the y direction can be determined as follows (*SI Appendix*):

$$K_y(\phi,\theta_0) \equiv K = \left.\frac{dF_y}{d\theta_2}\right|_{\theta_0} \text{ with } F_y = \frac{dU/d\theta_2}{dl/d\theta_2}. \quad [6]$$

Fig. 2*C* plots the numerical solution of the normalized stretching stiffness K/k as a function of the folding angle θ_2 for different inclined angle ϕ. At the initial state of $\theta_2 = 0$ without folding, it shows an infinity stiffness, representing a singularity state. As it starts to fold, the stiffness drops dramatically. For small angle of

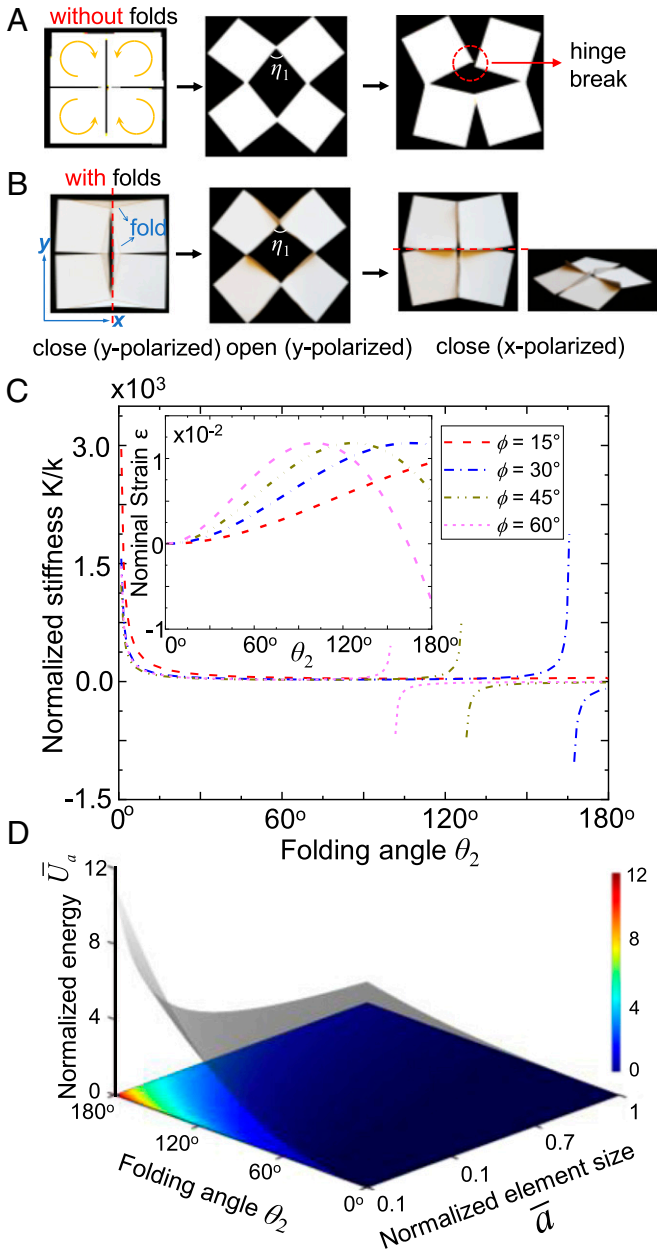

Fig. 2. Geometry and deformation of square-cut–based kirigami sheets with folds. (*A* and *B*) Comparison of shape shifting between a square-cut paper kirigami unit cell without (*A*) and with folds (*B*). Folding leads to the polarization switch and the reclosing of pores upon complete folding. (*C*) Theoretical predicted normalized stretching stiffness K/k at $\bar{d}$ = 0.75. *Inset* is the corresponding nominal strain. (*D*) Normalized energy as a function of normalized element size and folding angle to actuate the kirigami metasheet.

ϕ less than ϕ_c (e.g., ϕ = 15°), K/k decreases dramatically to a small positive plateau value. However, for $\phi \geq \phi_c$ (e.g., ϕ > 30°), it exhibits a second stiffness singularity at the transition folding angle θ_t with the peak strain as shown in the Fig. 2 *C*, *Inset*. Geometrically, such a singularity state represents a special configuration, where the diagonals of the rotated cut plates become aligned with the stretching direction. Mechanically, it indicates the transition point for the onset of a polarized direction switch. We find that a larger ϕ leads to an earlier transition at a relatively smaller folding angle. When beyond the transition point, the stiffness switches to be negative and decreases to a plateau, even to a zero value for $\phi \geq 45°$ upon further folding, indicating the reclosing of the pores. The singularity makes it challenging to realize the geometrically allowable shape transformation beyond the mechanically locked state, which is also one of the limitations through mechanical actuation for shape shifting (9, 20).

To address the challenge, we employ an alternative approach to reconfigure the kirigami metasheet beyond the maximally stretched state via remote thermal actuation by making all of the creases active. Correspondingly, the rotation of each cut unit can be remotely actuated by self-folding of connecting hinges at the creases, thus avoiding the singularity issue through mechanical loading (9, 20). For a periodic square kirigami metasheet with length of L composed of a number of N square unit cells, the required normalized actuation energy for in-plane transformation $\bar{U}_a = U_a/kL$ is given by $\bar{U}_a = \bar{U}/\bar{a} = 2N^{\frac{1}{2}}\bar{U}$, with $\bar{a} = a/L$ being the normalized size of the square element and $\bar{U} = (1-\bar{d})[(\theta_2-\theta_0)^2 + (\alpha-\alpha_0)^2/\cos\phi]$. Fig. 2*D* shows that $\bar{U}_a$ is inversely proportional to the normalized element size and increases parabolically with the folding angle. As expected, a smaller element size, equivalently larger number of elements, requires a higher actuation energy.

Meanwhile, the remote actuation will allow for active and individual control of each crease in both single-unit and periodic metasheets for either in-plane or out-of-plane rotation, enabling potential applications in stimuli-responsive kirigami machines that will be discussed later. It should be noted that the governing principle of the shape transformation via geometric models still applies here since it is independent of the actuation mechanism. The folding angle in the geometric model will be tuned by the self-folding at the active creases as discussed below.

Actuation of 2D Kirigami Metasheets. Rather than a single layered sheet, we use a thin sheet of trilayer composite model system to actuate the shape transformation in the 2D kirigami metasheets through mechanics and geometry-guided self-folding of active creases. As schematically illustrated in Fig. 3*A*, the top and bottom layer have the same thickness and are composed of the same nonactive materials, while the middle layer is made of active materials to allow expanding or shrinking in response to external stimuli. Then we introduce a cut to both sides to break its deformation symmetry.

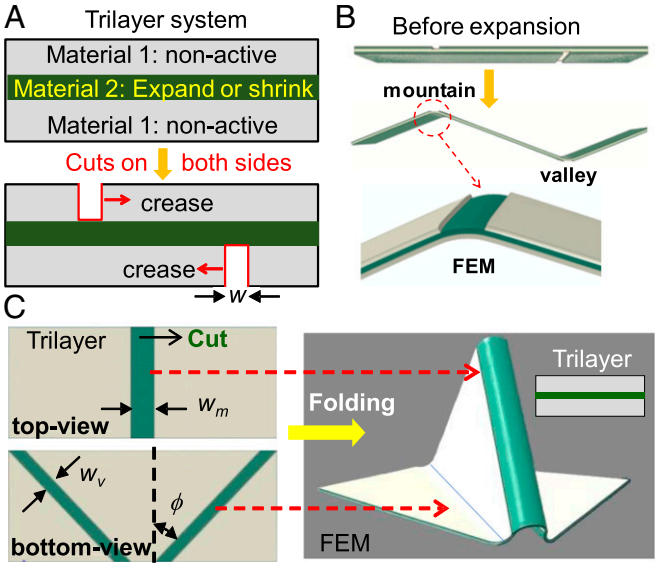

Fig. 3. Actuation through trilayer kirigami composite system. (*A*) Schematic of actuating directional folding in a trilayer thin sheet composite system through cut-induced symmetry breaking. (*B*) Corresponding proof-of-concept FEM simulation result. Two cuts are introduced to the top and bottom layer, respectively. Expansion of middle layer leads to the self-folding into a 3D *Z* shape. (*C*) FEM simulation on self-folding of the 3D hinge with 1 cut on the top and 2 inclined cuts on the bottom (ϕ = 45° and $w_v = w_m/2$).

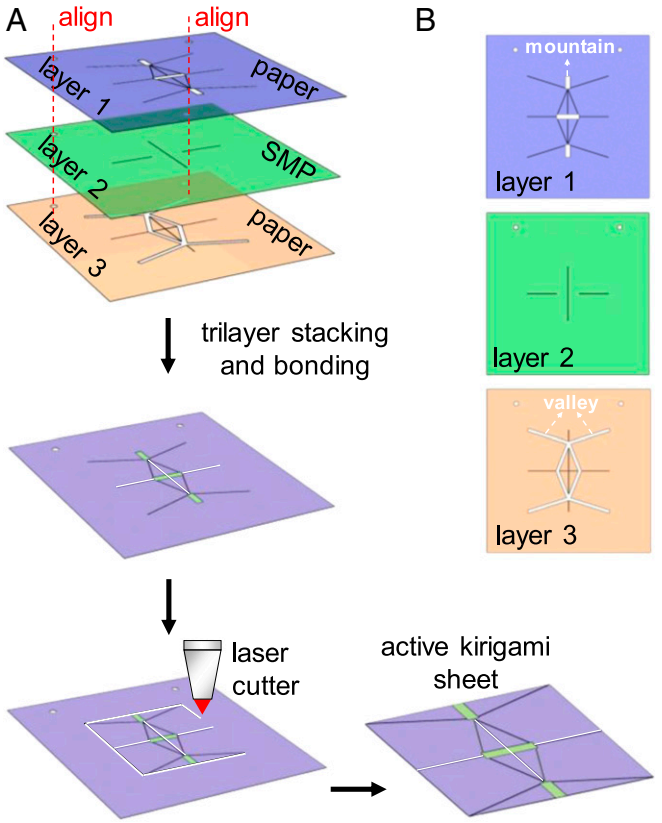

Fig. 4. Schematic of fabrication of an active kirigami metasheet. (*A*) Fabrication steps: stacking and bonding 3 layers (paper-SMP-paper) with prepatterned cuts in each layer shown in *B*. The 2 holes in each layer are used to align the 3 layers through alignment pins. Removing the supporting structures through a laser cutter generates the designed square cut unit.

The cuts enable and guide the directional bilayer bending at the cut region, playing the role as active creases. As demonstrated in the proof-of-concept finite-element method (FEM) simulation in Fig. 3*B*, as temperature increases, the trilayer sheet self-folds into a 3D *Z* shape along the cuts through bilayer bending (Fig. 3*B*). The folding angle at the creases can be well manipulated by the linear relationship with the cut width w in terms of the experimentally validated bimetal folding model (31) (*SI Appendix*, Figs. S6 and S7). The cut-based active creases can be further extended to design a self-folded 3D tetrahedron hinge in the trilayer composite (Fig. 3*C*), where the vertical cut (cut width w_m) on the top layer exposes the middle layer highlighted by dark green color and acts as an active mountain crease, and the 2 inclined cuts with inclined angle ϕ (cut width w_v) on the bottom layer act as active valley creases. $w_m = 2w_v$ is set to satisfy Eq. **2** to keep the cut plates coplanar after folding.

Next, we examine its application to actuate the shape transformation in 2D trilayer composite sheets with patterned square arrays of cuts through shape memory polymer (SMP)-based prototypes. Fig. 4*A* shows the schematic of fabricating the trilayer prototype in a single square unit cell (*SI Appendix*), where SMP-based shrink paper is sandwiched by 2 pieces of nonresponsive paper sheet with prepatterned cuts through a laser cutter. The shrink paper is composed of prestrained polystyrene, a type of SMP that shrinks in-plane upon heating above its glass transition temperature (15). The cuts in layer 1 and layer 3 define the mountain and inclined valley creases with cut widths of $w_m = 2w_v$, respectively, and layer 2 defines the through-thickness cuts (Fig. 4*B*). Stacking the 3 layers through double-sided silicone tape bonding and alignment pins forms a temperature-responsive kirigami sheet. At the vertices of cuts throughout the trilayer thickness, 1 mountain and 2 valley active creases based on cuts will form a self-folding tetrahedron hinge for structure reconfiguration.

The design is first examined by the FEM model of a single square unit cell with different inclined angles of ϕ. Fig. 5*A* shows the top view of the cut design with $\phi = 45°$. Upon temperature increase, the middle layer shrinks, and folding of creases at cuts leads to the rotation of the square cut units, thus the opening of the cuts into a rhombus pore shape. When it is fully folded with $\theta_2 = 180°$, the opening angle η_1 in the unit cell becomes ~90°, which is consistent with the geometrical model. The simulation result agrees well with the corresponding proof-of-concept SMP-based prototype shown in Fig. 5*A*′, where 4 cut plates are coplanar and show the same $\eta_1 = 90°$ with $\phi = 45°$ upon heating-induced self-folding of cut-based hinges. The circular holes are used to reduce the stress concentration to facilitate the self-folding. Guided by the design for polarization switch, we further increase ϕ to $\phi = 75°$; after actuation, as expected, both FEM simulation and experiment show that, as folding increases, the structure expands first and then shrinks to a compact state by reclosing the line cut in the middle with a switched polarization (Fig. 5 *B* and *B*′, and *SI Appendix*, Fig. S8*A*). Similar excellent agreement is also observed in the actuation of single unit cell with triangular cuts for either maximum opening of the line cuts into a hexagonal shape ($\phi = 60°$, *SI Appendix*, Fig. S9 *A* and *A*′ and Movie S2) or polarized switched shape with reclosed cuts after actuation ($\phi = 70°$, *SI Appendix*, Figs. S8*B* and S9 *C* and *C*′ and Movie S3), as well as in the corresponding kirigami metasheet composed of multiple periodic unit cells in both maximum opening (Fig. 5 *C* and *C*′, *SI Appendix*, Fig. S9 *B* and *B*′, and Movies S4 and S5) and polarized switch through pore reclosing (*SI Appendix*, Fig. S9 *D* and *E* and Movies S6 and S7).

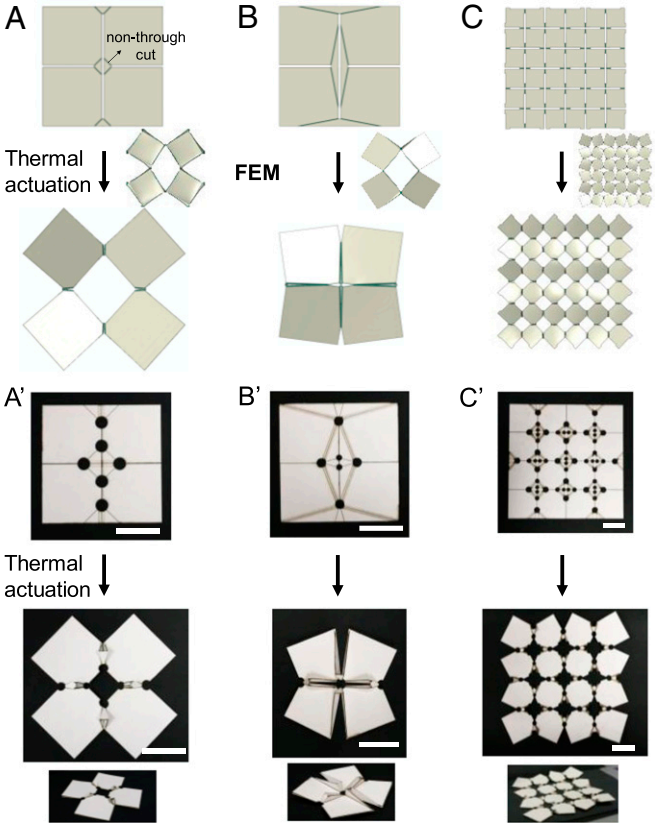

Fig. 5. Thermal actuation of 2D active kirigami metasheet. (*A*–*C*) FEM simulation results on thermal actuation of both a single kirigami unit cell (*A* and *B*) and periodic multiple unit cells (*C*) before and after complete folding of the mountain creases (i.e., $\theta_2 = 180°$). (*A*′–*C*′) Corresponding proof-of-concept experiments in actuating fabricated trilayer kirigami composite sheets. Larger inclined angle ϕ of valley creases leads to a polarization switch and reclosing of line cuts (*B* and *B*′) after complete folding. The preset values of ϕ are $\phi = 45°$ (*A*, *A*′, *C*, and *C*′) and 77° (*B* and *B*′). (Scale bar for all figures, 20 mm.)

Design and Actuation of 3D Kirigami Structures. When the folding angles at mountain ($\theta_2 \neq \theta_5$) and valley creases ($\theta_1 = \theta_3 \neq \theta_4 = \theta_6$) at the hinges (Fig. 6*A*) do not satisfy Eqs. **1** and **3**, the constraint on coplanar folded cut plates will be released. It allows the relative out-of-plane rotation between the hinged plates in the unit cell and thus enables multiple DOFs. For the square cut unit cell, it has 2 DOFs characterized by the 2 dihedral folding angles η_2 and η_3 between the 3 rigid square cut units as defined in Fig. 6*B*. From the geometry, we have the following:

$$\eta_2 = 2\theta_1 - \theta_2, \quad \eta_3 = 2\theta_4 - \theta_5, \qquad [7]$$

where $\eta_2 \in [-2\cos^{-1}(\tan\xi/\tan\phi), 2\cos^{-1}(\tan\xi/\tan\phi)]$ and $\eta_3 \in [-2\cos^{-1}(\tan\xi'/\tan\phi), 2\cos^{-1}(\tan\xi'/\tan\phi)]$ with $\xi' = \sin^{-1}[\sin\phi\cos(\theta_5/2)]$. The positive and negative signs of η_2 and η_3 in Eq. **7** represent folding-up and folding-down of the 2 neighboring hinged plates, respectively (Fig. 6*B*).

As schematically illustrated in the Fig. 6 *C–F*, *Insets*, the combination of positive and negative η_2 and η_3 represents 4 basic out-of-plane deformation modes in terms of their relative folding directions, i.e., mode I ($\eta_2 > 0, \eta_3 > 0$), mode II ($\eta_2 < 0, \eta_3 < 0$), mode III ($\eta_2 < 0, \eta_3 > 0$), and mode IV ($\eta_2 > 0, \eta_3 < 0$). Correspondingly, in the prototypes of trilayer SMP-based composite sheet, guided by *SI Appendix*, Eq. **S8** and Eq. **7**, we can manipulate the folding angle at each mountain and valley crease by tuning the cut width in the unit cell, thus to achieve the 4 basic 3D configurations programming from self-folding of the same planar square cut unit cell, as shown in Fig. 6 *C–F*. The design principle in the single cut unit cell can be readily extended to multiple periodic units to program different actuated 3D kirigami sheets from the same cut pattern. Fig. 6*G* shows an example of a 2D trilayer sheet consisting of 4 square cut unit cells. Through active hinge controlled dihedral folding and relative rotation of cut plates in both unit cells and connections between units, the 2D metasheet with the same square-cut pattern can self-fold into distinct 3D expanded and compact structures, e.g., a 3D pop-up lattice-like structure through combining mode II in the unit cell and mode I in connecting the unit cells (Fig. 6*H* and Movie S8), a dome-like shell structure by only allowing single mode II in both unit cells and their connections (Fig. 6*I* and Movie S9), and a corrugated and compact 3D structure by manipulating mode IV (Fig. 6*J*).

Fig. 6*K* shows that the self-folded 3D kirigami metastructures demonstrate distinct compression capacity. The 3D lattice-like structure exhibits a dramatic strain-hardening behavior and the highest compression stiffness, which are attributed to the dominated compression deformation in the supporting rigid square-cut plates. The corrugated structure shows a moderately strain-hardening behavior, which is much more compliant due to the combined bending and folding of the hinges and compression of the cut units. In sharp contrast, due to the shallow feature of the dome-like structure, it shows the lowest loading capacity and the whole structure becomes flattened upon further compression. The demonstrated distinct mechanical properties of self-folded 3D kirigami structures arise from programmable combination of different deformation modes of hinge bending or plate compression in the unit cell, allowing the potential applications of kirigami structures as structural materials beyond the interest of high stretchability and shape morphing (8, 9, 17–22). It should be noted that despite the similar strategy for generating 3D structures from folding of kirigami sheets with combined folds and cuts by Sussman et al. (29), the shape shift mechanisms are on the contrary: Sussman et al. leverage folds to close the initially excised hexagonal holes in a flat kirigami sheet, which generates nonporous compact 3D step-like structures from a porous kirigami sheet (29). By contrast, our work utilizes folding to open and even reclose the slits in a nearly nonporous kirigami sheet. It is beyond the inverse problem to Sussman et al.'s work since it achieves both expandable and compact structures in both 2D and 3D, which are challenging to be realized in porous kirigami sheets through folding-induced closing of pores and self-folding of origami (12–16).

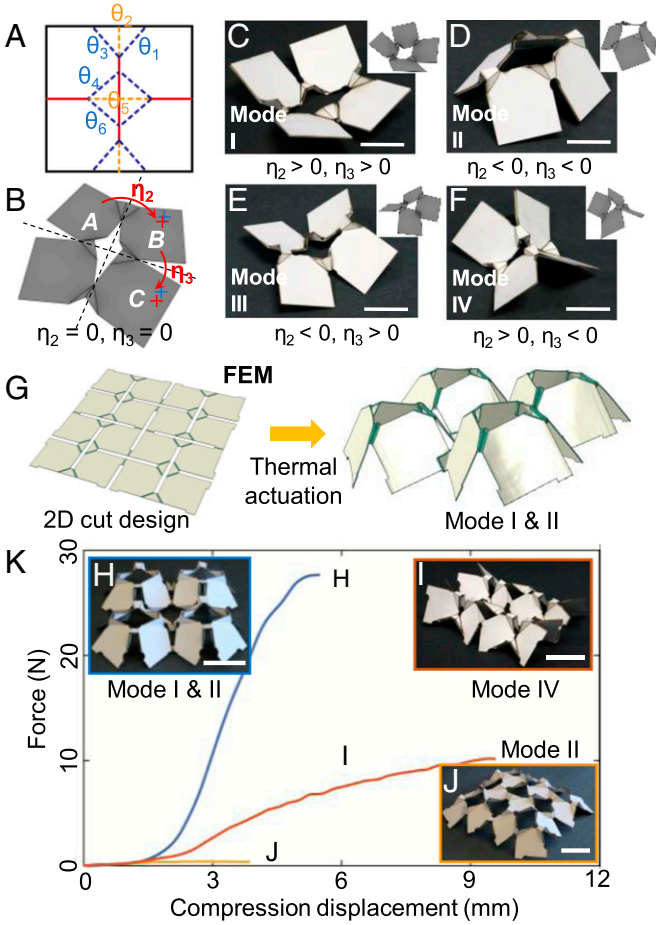

Fig. 6. Thermal actuation of 3D kirigami metastructures. (*A* and *B*) Schematics on different folding angles at creases leading to relative out-of-plane rotation (η_2 and η_3) between 4 cut plates. (*C–F*) Demonstration of thermally actuated 4 basic out-of-plane deformation modes in the unit cell through trilayer (paper–SMP–paper) thin sheets. The *Top Right* shows the schematic of deformation modes. (*G*) Simulated 3D pop-up kirigami lattice structure from a planar kirigami sheet upon thermal actuation. (*H–J*) Prototypes of programmable self-folded 3D kirigami metastructures from the same planar kirigami sheets through combining different deformation modes. (*K*) Corresponding measured force-displacement curves of the metastructures under compression. (Scale bar for all figures, 20 mm.)

Potential Applications as Programmable Kirigami Machine. To illustrate the utility of the multi-DOF in the cut unit cell, we explore the design of simple programmable self-folding kirigami machines by attaching 4 self-folding "arms" to the same square cut unit cell in the center. Fig. 7*A* shows the top view of the prototype made of the trilayer SMP-based composite kirigami sheet. The sheet is patterned with cuts on both sides acting as either active mountain or valley folds shown in Fig. 7 *A*, *i–v*, for programmable 3D shape shifting. By combining directional self-folding in the 4 arms and multi-deformation modes in the center square cut unit cell through cuts, guided by FEM simulation (Fig. 7*B*), we demonstrate that the same cut design can be programmed into a variety of self-folded kirigami machines (Fig. 7*C*), including the water spider-like shape (mode II with $\eta_2 < 0, \eta_3 < 0$), soft crawler-like shape (32) (mode I with $\eta_2 > 0, \eta_3 > 0$), crab claw-like shape (mode IV with $\eta_2 > 0, \eta_3 < 0$), gripper-like shape ($\eta_2 = 0, \eta_3 = 0$), and closed box-like shape ($\eta_2 = 90°, \eta_3 = 0$). Both simulation and prototypes show good agreement for all of the actuated 3D shapes through cuts-guided self-folding (Fig. 7*C*).

By harnessing the in-plane rotation in the square cut unit cell, i.e., $\eta_2 = 0, \eta_3 = 0$, we demonstrate proof-of-concept experiments in design of a thermally actuated kirigami gripper (Fig. 7*D* and Movie S10) and a kirigami soft robot making turns easily (Fig. 7*E* and Movie S11). Upon raising the temperature, the square cut unit in the center of the kirigami sheet as seen in Fig. 7*D* starts to rotate in-plane

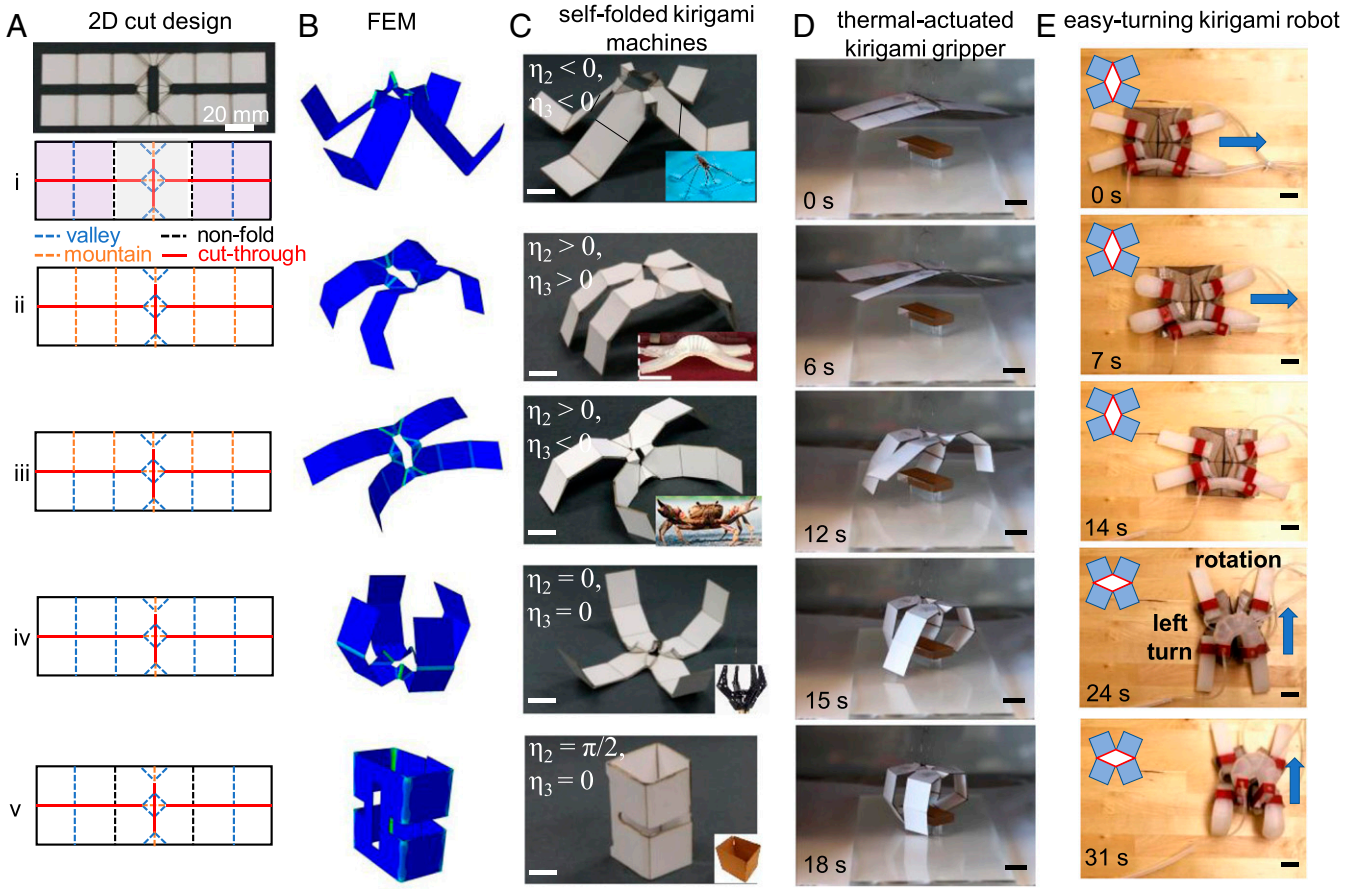

Fig. 7. Programmable kirigami machines. (*A*–*C*) Programmable thermal actuated 3D kirigami structures from the same cut design in trilayer composite sheets by manipulating different 3D deformation modes of the square kirigami unit in the center. (*A*) Schematics of designed folds and cuts. (*B* and *C*) FEM simulation results and experimental prototypes of thermal actuated 3D kirigami machines. (*D*) Demonstration of a thermal actuated kirigami gripper. (*E*) Demonstration of a kirigami crawler making turns easily by harnessing the polarization switch in the kirigami square cut unit with folds. (Scale bar for all figures, 20 mm.)

to open the cut, which drives the initially closed 4 "fingers" to rotate and become apart from each other, followed by the downward folding of each finger at 2 joints. Further folding at the fingers' joints results in the closing of 4 folded fingers for potential weight lift (Movie S10). Simple geometrical model on the grasping radius R (*SI Appendix*, Fig. S10*A*) shows that R decreases monotonically with both the folding angle of the finger joint and the opening angle η_1 of the square cut unit (*SI Appendix*, Fig. S10*B*). Thus, when both the finger joints bend to their maximum folding angle ~90° and the square rotates to its maximum opening angle with $\eta_{1\max} = 2\phi = 90°$ in the studied model system, the kirigami gripper achieves the minimum grasping radius $R_{\min}$ with a theoretical value of $R_{\min} \sim 0.15a = 3.75$ mm ($a = 25$ mm) (*SI Appendix*, Fig. S10*C*), which is close to the measured $R_{\min} \sim 4.5$ mm in the prototype. Similarly, by replacing the 4 fingers in the gripper with 4 pneumatic bending "legs," we integrate the paper square cut unit as "skeleton" with soft bending actuators as "muscle" for an easy-maneuvering soft robot (Fig. 7*E* and Movie S11). The sequential pneumatic actuation in the 4 bending legs leads to the crawl along the horizontal direction. Upon pneumatic actuation on the connected bending actuator on the bottom, it can easily drive the polarization switch in the single DOF cut unit with a preset large inclined angle of $\phi = 70°$; consequently, it switches its walking gait to be along the vertical direction, thus making a left turn to move vertically upon pneumatic actuation.

Discussion and Conclusions

Despite the introduced additional large number of folds in the reconstructed kirigami metasheet, the control of self-folding guided structural reconfiguration in both single unit and a periodic structure through thermal actuation is still applicable. Here, based on the geometrical and minimum energy constraint, we propose a theoretical framework to explore the governing equations between the input (i.e., temperature) and outputs (i.e., folding angles) for potential control applications in thermal actuation of kirigami metasheets and machines.

For a single square cut unit cell, despite a number of 12 folds, it has only 2 DOFs by considering the symmetry, i.e., θ_1 and θ_4 or θ_2 and θ_5 (*SI Appendix*). Such 4 folding angles are not independent. The folded 3D structure configuration is represented by the folding angle θ_i at each fold (*SI Appendix*, Fig. S11*A*), which are constrained by the closed strip of facets (*SI Appendix*, Fig. S11*B*), i.e., the transformation along the strip should satisfy $\chi_1\chi_2\cdots\chi_{11}\chi_{12} = I$, where 4×4 matrices χ_i represent rotation and translation of the loop and I is the identity matrix (*SI Appendix*). From the geometric constrained loop, the relationship between the folding angles can be obtained as below:

$$(\cos\theta_1 - \cos\theta_4)(1-\bar{d}) = (\cos\theta_2 - \cos\theta_5)\left(\bar{d} - \bar{\phi}\right), \quad [8]$$

$$\cos\phi\sin\theta_1 + \sin\theta_2 = \cos\phi\sin\theta_4 + \sin\theta_5/\sin\phi, \quad [9]$$

where $\bar{\phi} = \tan\phi/(1+\tan\phi)$. From the perspective of elastic energy, under thermal actuation, the unit cell will settle to a 3D folded configuration that minimizes its elastic energy through the

competition between bending energy of the folds (*SI Appendix*), which gives the following:

$$\begin{aligned}(m_1T-\theta_1)/(m_2T-\theta_2)&=\kappa_1(T)\sqrt{\cos\phi},\\(m_4T-\theta_4)/(m_5T-\theta_5)&=\kappa_2(T)\sqrt{\cos\phi},\end{aligned}\qquad[10]$$

where T is the actuation temperature, m_i is the linear constant of the temperature-angle function in *SI Appendix*, Eq. **S15**, and κ_i is the temperature-related constant for fold i. Based on Eqs. **8**–**10**, the 4 correlated folding angles governing the folded configuration of the square cut unit cell can be determined through controlling the input of T. The nonlinear governing equations can be numerically solved using the Newton's method, where a unique solution can be achieved through the interval analysis of the Newton's method (*SI Appendix*). When connecting the unit cells in a periodic way, their deformation should satisfy the additional deformation compatibility condition when crossing the unit cells. The periodic structure is constrained by the following equations:

$$\eta_2^{(i,j)}=\eta_2^{(i+1,j)},\quad \eta_3^{(i,j)}=\eta_3^{(i,j+1)},\qquad[11]$$

where i and j are the respective row and column number of the unit cell in the periodic structure. For the 4 basic deformation modes in a square cut unit cell, there are 9 types of combinations (*SI Appendix*, Fig. S12). The unit cells can be connected by 4 types of connections, corresponding to the shapes of mode I/III, mode I/IV, mode II/III, and mode II/IV, respectively. Each type of connection can deform between 2 shapes to enrich the library of 3D structure reconfigurations.

In conclusion, we demonstrate a strategy that combines cuts and folds to reconfigure kirigami metamaterials with more DOFs than sole cuts through folding-induced opening and reclosing of cuts. The implemented folds release the constrained DOF of planar hinges at cut tips to allow both in-plane and out-of-plane rotation at the hinges. Such a design not only enriches a library of shape shifting of kirigami metasheets in both 2D and 3D, but also facilitates more freedom in thermal actuation of self-folded programmable kirigami metastructures and soft machines.

Due to the irreversibility of SMP used in composite sheets, the demonstrated structural reconfigurations cannot be reversed through unfolding of creases. The proposed design principles reported here, however, can be applied to other active materials systems with micrometer-sized resolution for reversible deformation, e.g., by replacing the sandwiched materials with pH- or temperature-responsive hydrogels (13), or temperature- or light-responsive liquid crystal elastomers (33, 34) with double-side coated nonactive stiff polymers, or graphene-glass–based multilayer microstructures (35). Despite the scale independency of the design principle, more precise fabrication methods are needed for small-scale kirigami, e.g., via chemical etching, focused ion beam, or e-beam lithography for line cuts or creases, followed by deposition of active materials at creases. For practical applications of kirigami-based machines in soft robotics, integration of the responsiveness with other functions, such as sensing and control will be critically important. The augmented DOF in both deformation and actuation from the foldable hinges will open venues for potential applications in programmable active matter, adaptive building envelopes, reconfigurable kirigami soft robots, and micromachines.

Materials and Methods

Details of fabrication of active trilayer kirigami sheets, finite-element simulation, and mechanical testing are described in *SI Appendix*.

Data and Materials Availability. All data needed to support the conclusions are presented in the main text or *SI Appendix*.

ACKNOWLEDGMENTS. J.Y. acknowledges the funding support from the National Science Foundation (CAREER-1846651 and CMMI-1727792).

1. J. Christensen, M. Kadic, O. Kraft, M. Wegener, Vibrant times for mechanical metamaterials. *MRS Commun.* **5**, 453–462 (2015).
2. A. A. Zadpoor, Mechanical meta-materials. *Mater. Horiz.* **3**, 371–381 (2016).
3. M. Schenk, S. D. Guest, Geometry of Miura-folded metamaterials. *Proc. Natl. Acad. Sci. U.S.A.* **110**, 3276–3281 (2013).
4. J. L. Silverberg *et al.*, Applied origami. Using origami design principles to fold reprogrammable mechanical metamaterials. *Science* **345**, 647–650 (2014).
5. E. T. Filipov, T. Tachi, G. H. Paulino, Origami tubes assembled into stiff, yet reconfigurable structures and metamaterials. *Proc. Natl. Acad. Sci. U.S.A.* **112**, 12321–12326 (2015).
6. Z. Zhai, Y. Wang, H. Jiang, Origami-inspired, on-demand deployable and collapsible mechanical metamaterials with tunable stiffness. *Proc. Natl. Acad. Sci. U.S.A.* **115**, 2032–2037 (2018).
7. Y. Tang *et al.*, Design of hierarchically cut hinges for highly stretchable and reconfigurable metamaterials with enhanced strength. *Adv. Mater.* **27**, 7181–7190 (2015).
8. M. Eidini, G. H. Paulino, Unraveling metamaterial properties in zigzag-base folded sheets. *Sci. Adv.* **1**, e1500224 (2015).
9. Y. Tang, J. Yin, Design of cut unit geometry in hierarchical kirigami-based auxetic metamaterials for high stretchability and compressibility. *Extreme Mech. Lett.* **12**, 77–85 (2017).
10. Y. Tang *et al.*, Programmable kiri-kirigami metamaterials. *Adv. Mater.* **29**, 1604262 (2017).
11. N. Yang, J. L. Silverberg, Decoupling local mechanics from large-scale structure in modular metamaterials. *Proc. Natl. Acad. Sci. U.S.A.* **114**, 3590–3595 (2017).
12. E. Hawkes *et al.*, Programmable matter by folding. *Proc. Natl. Acad. Sci. U.S.A.* **107**, 12441–12445 (2010).
13. J.-H. Na *et al.*, Programming reversibly self-folding origami with micropatterned photo-crosslinkable polymer trilayers. *Adv. Mater.* **27**, 79–85 (2015).
14. T. T. Michael *et al.*, Self-folding origami: Shape memory composites activated by uniform heating. *Smart Mater. Struct.* **23**, 094006 (2014).
15. Q. Zhang *et al.*, Origami and kirigami inspired self-folding for programming three-dimensional shape shifting of polymer sheets with light. *Extreme Mech. Lett.* **11**, 111–120 (2017).
16. Y. Liu, B. Shaw, M. D. Dickey, J. Genzer, Sequential self-folding of polymer sheets. *Sci. Adv.* **3**, e1602417 (2017).
17. A. Rafsanjani, K. Bertoldi, Buckling-induced kirigami. *Phys. Rev. Lett.* **118**, 084301 (2017).
18. Y. Zhang *et al.*, A mechanically driven form of kirigami as a route to 3D mesostructures in micro/nanomembranes. *Proc. Natl. Acad. Sci. U.S.A.* **112**, 11757–11764 (2015).
19. A. Rafsanjani, L. Jin, B. Deng, K. Bertoldi, Propagation of pop ups in kirigami shells. *Proc. Natl. Acad. Sci. U.S.A.* **116**, 8200–8205 (2019).
20. Y. Cho *et al.*, Engineering the shape and structure of materials by fractal cut. *Proc. Natl. Acad. Sci. U.S.A.* **111**, 17390–17395 (2014).
21. Y. Yang, M. A. Dias, D. P. Holmes, Multistable kirigami for tunable architected materials. *Phys. Rev. Mater.* **2**, 110601 (2018).
22. S. Yang, I.-S. Choi, R. D. Kamien, Design of super-conformable, foldable materials via fractal cuts and lattice kirigami. *MRS Bull.* **41**, 130–138 (2016).
23. M. K. Blees *et al.*, Graphene kirigami. *Nature* **524**, 204–207 (2015).
24. T. C. Shyu *et al.*, A kirigami approach to engineering elasticity in nanocomposites through patterned defects. *Nat. Mater.* **14**, 785–789 (2015).
25. Y.-S. Guan, Z. Zhang, Y. Tang, J. Yin, S. Ren, Kirigami-inspired nanoconfined polymer conducting nanosheets with 2000% stretchability. *Adv. Mater.* **30**, e1706390 (2018).
26. A. Lamoureux, K. Lee, M. Shlian, S. R. Forrest, M. Shtein, Dynamic kirigami structures for integrated solar tracking. *Nat. Commun.* **6**, 8092 (2015).
27. A. Rafsanjani, Y. Zhang, B. Liu, S. M. Rubinstein, K. Bertoldi, Kirigami skins make a simple soft actuator crawl. *Sci. Robot.* **3**, eaar7555 (2018).
28. R. M. Neville, F. Scarpa, A. Pirrera, Shape morphing kirigami mechanical metamaterials. *Sci. Rep.* **6**, 31067 (2016).
29. D. M. Sussman *et al.*, Algorithmic lattice kirigami: A route to pluripotent materials. *Proc. Natl. Acad. Sci. U.S.A.* **112**, 7449–7453 (2015).
30. Z. Y. Wei, Z. V. Guo, L. Dudte, H. Y. Liang, L. Mahadevan, Geometric mechanics of periodic pleated origami. *Phys. Rev. Lett.* **110**, 215501 (2013).
31. S. Timoshenko, Analysis of Bi-metal thermostats. *J. Opt. Soc. Am.* **11**, 233–255 (1925).
32. R. F. Shepherd *et al.*, Multigait soft robot. *Proc. Natl. Acad. Sci. U.S.A.* **108**, 20400–20403 (2011).
33. Y. Xia, G. Cedillo-Servin, R. D. Kamien, S. Yang, Guided folding of nematic liquid crystal elastomer sheets into 3D via patterned 1D microchannels. *Adv. Mater.* **28**, 9637–9643 (2016).
34. E. Bukusoglu, M. Bedolla Pantoja, P. C. Mushenheim, X. Wang, N. L. Abbott, Design of responsive and active (soft) materials using liquid crystals. *Annu. Rev. Chem. Biomol. Eng.* **7**, 163–196 (2016).
35. M. Z. Miskin *et al.*, Graphene-based bimorphs for micron-sized, autonomous origami machines. *Proc. Natl. Acad. Sci. U.S.A.* **115**, 466–470 (2018).